LÊ NGỌC TÚ

RESEARCH, DESIGN AND FABRICATION OF MICROFLUIDIC DEVICE INTEGRATING MIXTURE MODULE AND MAGNETIC NANOPARTICLE TRAPPING MODULE FOR BIOMEDICAL ANALYSIS APPLICATION.

Major: Solid Physics

Code: 9 44 01 04

SUMMARY OF PHYSICS DOCTORAL THESIS

Công trình được hoàn thành tại: Học viện Khoa học và Công nghệ - Viện Hàn lâm Khoa học và Công nghệ Việt Nam.

Người hướng dẫn khoa học 1: GS. TS. Trần Đại Lâm

Người hướng dẫn khoa học 2: TS. Cao Hồng Hà

Phản biện 1: …
Phản biện 2: …
Phản biện 3: ….

Luận án sẽ được bảo vệ trước Hội đồng đánh giá luận án tiến sĩ cấp Học viện, họp tại Học viện Khoa học và Công nghệ - Viện Hàn lâm Khoa học và Công nghệ Việt Nam vào hồi … giờ ..', ngày … tháng … năm 2023

Có thể tìm hiểu luận án tại:
    - Thư viện Học viện Khoa học và Công nghệ
    - Thư viện Quốc gia Việt Nam

INTRODUCTION

1. The necessary of the thesis topic

Currently, the term "microfluidics" refers to systems containing channels and chambers with a width and height between 100 nm and 1000 μm and a length depending on the intended use (up to several tens of cm). This area of research in device systems allows the implementation of new functions and the study of phenomena that are difficult to perform in large devices. The crucial outstanding characteristic of microfluidic systems is the interaction between objects and fluids at the microscopic level inside the microzones of the devices. These effects are expected to produce many advantages, such as faster reaction times and simple fluid dynamics.

Furthermore, microfluidic systems combined with microelectronics or microsensors will provide integrated microfluidic devices that meet the miniaturization trend's requirements. One of the essential applications of microfluidic systems for biomedical analysis purposes is the integration of functional modules at the laboratory scale into microfluidic systems. It will allow all steps of an analytical procedure to happen in a single microfluidic device, the so-called "Lab-on-a-chip system" that makes the fabrication of microchannels more and more suitable for different applications in chemistry, biology, and medicine.

Based on those reasons, the topic of the thesis was chosen as following: "*Research, design and manufacture a microfluidic device with integrated module for mixing and trapping nanoparticles from biomedical analysis application*".

2. The goals of the thesis

- To fabricate a microfluidic device integrating functional modules: mixing of material fluids and trapping magnetic particles using a flat electromagnet built inside a channel of the microfluidics.

- To fabricate a microfluidic chip system coupled with an electrochemical sensor that can perform analysis of antibiotic residues in livestock treatment.

3. The major contents of the thesis:

Content 1: Study on the design, fabrication, and package of a microfluidic chip with integrated nano-particle trapping module using planar coil system. The main contents include:

- Design of the overall structure of the microfluidic chip using high biocompatible polymer materials (Poly(dimethylsiloxane) – PDMS, Poly(methyl methacrylate) – PMMA) suitable for biological analysis requirements.

- Design and fabrication of a mixing module consisting of zigzag-shaped micro-channel, splitter, and stable flow area.
- Design and fabrication of a flow rate control valve system for the liquid pumped into the microfluidic system based on PDMS material.
- Design and fabrication of a nano-particle trapping module using planar coils (electromagnetic magnets), which are integrated into the microfluidic system and can be flexibly activated by the magnetic field through current control. It is easy to attach and remove from the microfluidic system.

Content 2: Design, fabrication, and completion of an integrated microfluidic device with a flat electrochemical sensor based on a printed carbon electrode (SPE) modified with advanced material system. The contents include:
- Fabrication of electrochemical sensor systems using advanced composite materials specifically for analyzing antibiotics in solutions through direct electrochemical synthesis on the electrode surface.
- Testing the amount of sulfomethaxazone antibiotics in T.T.S Nam Thai intestinal disease medicine from the Nam Thai Veterinary Pharmaceutical Company.
- Developing a technique to combine micro-channel with the subtrate of the integrated microfluidic electrochemical sensor system using mechanical structure, which allows the reuse of the micro-channel system and the printed carbon electrode.

CHAPTER 1. THE OVERVIEW

1.1. Microfluidics

Microfluidics has long been regarded as a significant area of technology with numerous distinguishing features from other fields. One may argue that the crucial historical turning point for microfluidic systems really happened in the 2000s. Microfluidics development is directly linked to the advancement of materials and processing techniques. In particular, the advancement of manufacturing techniques has guided the design and applications of microfluidic devices in a variety of disciplines, including biology, chemistry, and medicine.

1.2. Microfluidics in immunoassay using magnetic nanoparticles

The magnetic nanoparticles engage with the material streams (antigens, antibodies, etc.) during their migration through the channel and are trapped in a specific place by magnetic force, similar to the old ELISA approach. Antibodies and antigens immobilized onto the surface of magnetic nanoparticles will be recognized using various techniques such as fluorescence labeling or electrochemical analysis. Besides, the antibody can be immobilized on the particle surface outside of the microchannel.

Lin et al. used a particular probe antibody to bind negatively charged DNA fragments for signal amplification in a magnetic nanoparticle-based immunoassay. The manufactured microfluidic system includes an external magnetic field (magnet) positioned beneath the channel to retain the magnetic nanoparticles (120 nm) at the location of an integrated electrochemical microelectrode.

1.3. Introduction to microfluidics integrating with electrochemical sensors

Companies have created flat electrode systems (screen printed electrodes (SPE)) that combine three conventional electrodes: working electrode, counter/auxiliary electrode, and reference electrode, for obtaining the same purpose as an electrochemical analytical system. It is easy to integrate this kind of electronds into a microfluidic devices to perform an electrochemical analysis more convinently.

1.4. Overview of methods for detecting sulfonamide residues

Apart from the conventional methods currently used such as high-performance liquid chromatography, spectroscopy, electrochemistry, etc., among them, electrochemical methods have great potential to develop into methods with high reliability and sensitivity. Recent publications have focused on the use of nano materials, nanocomposites, conductive polymers and molecularly imprinted polymers (MIP) to modify working electrodes for selective detection of low-concentration sulfonamides. In fact, the use of nano materials allows for enhanced electrical signal and improved selectivity related to the sulfonamide oxidation process. In particular, graphene improves surface electron transmission of the electrode and therefore exhibits high catalytic properties. Therefore, they have been widely used in many applications.

## CHAPTER 2. FABRICATION PROCEDURE OF MICROFLUIDIC DEVIVES

Figure 3.1. General scheme of microfluidic devices fabrication

2.1. Design of micro-channel

Microchannels are designed using specialized vector drawing software Inkscape Ver. 1.2.2. Figure 2.2 shows the design of a typical mask using Inkscape software and printing on a polycarbonate sheet background.

Figure 2.2. Mask design for micro-channels using Inkscape software and printed on polycarbonate material. (a). The microchannel contains the mixing modulus and the magnetic nanoparticle trapping site. (b)-(c).
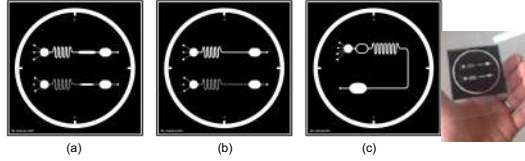
2.2. Microchannel fabrication

Figure 2.4 describes the mold fabrication process for microchannels using SU-8 3050 material as steps:

(a), (b): Spin-coating SU-8 photoresist on the substrate with a thickness of 50 μm (2 steps: Step 1- 500 rpm for 10 seconds with an acceleration of 100 rpm/s; Step 2- 3000 rpm for 30 seconds with an acceleration of 300 rpm).

(c): Soft baking the layer SU-8 on an electric stove at 95°C for 20 minutes.

(d): UV exposure with an irradiation

Figure 2.4. The fabrication process of SU-8 molds for micro-channels at the Nano and Energy Center, NEC.

energy of 200 mJ/cm² on a SU-8 layer to create an image according to the mask design. (e): Post baking to assist the UV irradiated image to be shaped and solidified, then the substrate is dried at 95°C for 4 minutes. (f), (g): Wash and create the mold (development), the SU-8 part that was not exposed to UV were dissolved in a special solvent (SU-8 developer) to obtain the shape of the mask. The substrate was washed twice: one was done in 7 minutes; the other (to replace the SU-8 developer solution) was carried out from 3 to 4 minutes depending on the actual circumstance. The substrate was then rinsed with iso-propanol and dried with N_2. Hard baking: this step is optional and can be skipped.
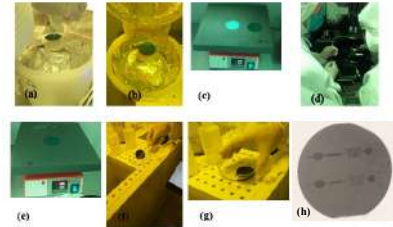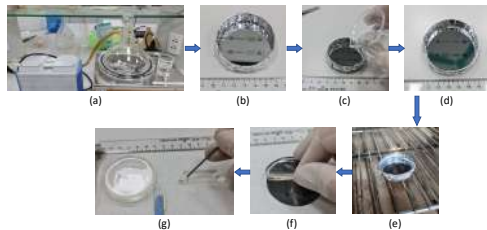
Figure 2.5. Microchannel fabrication procedure using a PDMS rapid prototyping technique

(a): PDMS was prepared by mixing two components in a 10:1 silicone elastomer/curing agent ratio.

The mixture was then stirred and defoamed by vacuum in a desicator. After de-foaming process, the homogenized mixture was poured onto the

surface of the mold in an adequate amount, depending on the required thickness of the PDMS layer (usually 4-6 mm thick). (b): Fix the mold (see above description) to the bottom of the plastic petri dish with special adhesive tape. It is also possible to wrap around the Petri dish with aluminum foil for easy separation of the channel and the substrate after finishing. (c): After the step of pouring PDMS onto the substrate, if air bubbles appear, the degassing step was done more. (d): Microscope was examined again to make sure no foam appearing in the mold parts. (e): The PDMS layer was completely cured at 90°C in 90 minutes. (f): The microchannels and the entire PDMS piece from the base were separated using a special knife. (g): The microchannel profile was cut and the channel holes for in and out were punched.

On each Si substrate (Figure 2.4.h) there were two types of molds for microchannels. Microchannel 1: total length was 3.2 cm; width × height of channel: 50× 500 μm; Microchannel 2: Total length: 3.2 cm; width height of channel: 50×250 μm.

2.3. Packaging microfluidic device and leaking test

The packging microfluidic system for the application is performed by the reversible technique, thanks to a mechanical structure that shown in Figure 2.7.
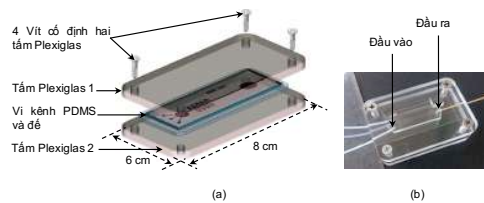

Figure 2.7. (a) Procedure for assempling the microchannel to the bottom subtrate by using a mechanical structure; (b) Completed microfluidic image.

Figure 2.10. The leaking test of the microfluidics assembled according to the mechanical assempling technique using two clamps of the Plexiglas® materials. (a). Experimental diagram; (b). Microfluidic system with inputs and outputs in this test.
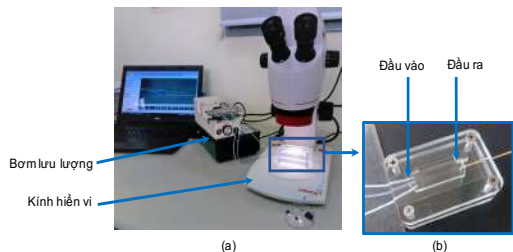
The leaking test of the microfluidic system after attaching to the mechanical structure is done as following steps: Three flows of distilled water are injected into the microfluidic system with three inputs and the

total flow rate varies from 100; 200; 300; 400 and 500 µL/min (using pump: RaZELTM R99-FMZ) and pumped continuously for 60 minutes, respectively, for each flow rate. Microfluidic systems are visually inspected for liquid leakage during testing to assess the fluid leakage and pressure resistance. Experimental diagram as shown in Figure 2.10.

CHAPTER 3. DESIGN AND FABRICATION OF FLUID CONTROL VALVE SYSTEM

3.1. Design and manufacture mechanical valve system using PDMS

The mechanical valve has a structure as shown in Figure 3.1, this valve uses a stop screw and is fixed with Plexiglas® and PDMS materials.


Figure 3.1. Design a valve system to control multiple fluid flows into a microfluidic system: (a) - (b) Valve cross-sections (at a control valve); (c) - (d) Detailed design of liquid multi-flow control device.
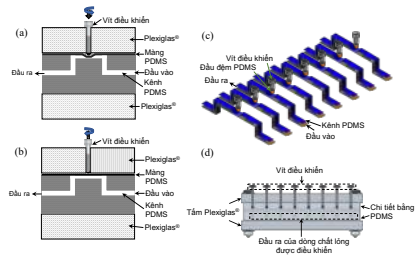
3.2. Liquid flow control test in microfluidic device

The experiment to investigate the mixing ability of three liquid flows in the microfluidics is depicted in Figure 3.5.


Figure 3.5. Experimental design to test the mixture ability and control the liquid flow of the control valve system.
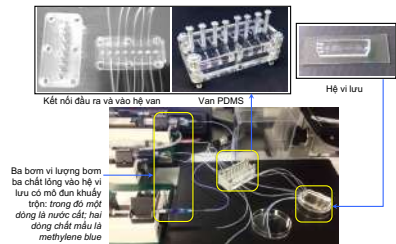
The mixing result of three liquid flows at the mixing module with the control of the liquid flow by the valve system is shown in Figure 3.6.

Figure 3.6. Test results of the three-fluid mixing process. (a), (b) mixing module, (c) liquid storage area.

These results show that the valve can operate stably in hundreds of opening/-closing or throttling cycles during the experiment in later parts of thesis. Response time 1 - 2 seconds; Fluid flow is flexibly controlled in opening/closing or throttling.
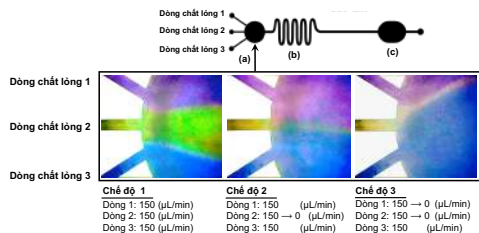
CHAPTER 4. DESIGN AND FABRICATION OF MICROFLUIDICS INTEGRATING MIXING AND NANOPARTICLE TRAPPING MODULES.

4.1. Computational/simulation model, design and fabrication of magnetic nanoparticle trapping module

4.1.1. Model for the magnetic field calculation of a planar coil

A current carrying conductor I produces a magnetic field strength H. The strength and direction of H depend on r, the distance from the current to the point P, Figure 4.1(a).

The magnetic field at any point P due to current can be calculated by adding up the magnetic field contributions, dH, from small segments of the wire dℓ. Biot – Savart law allows to calculate the magnetic field strength, dH generated by the current I.dℓ:

Figure 4.1. (a). Magnetic field strength H at point P caused by the current carrier element Idℓ. (b). Magnetic field strength H at point P caused by N elements I carry parallel currents.
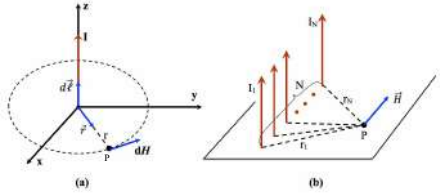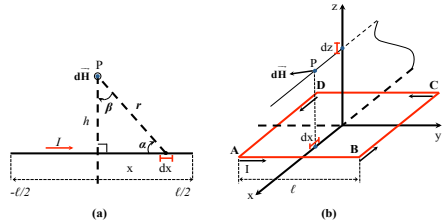

Figure 4.2. a. Magnetic field strength H at point P produced by a straight wire (a), and by a square coil (b). In which: I: amperage; h: distance from wire to point P; r: distance from wire to point P; ℓ: side length of the square turn.

$$dH = \frac{1}{4\pi} \frac{Id\boldsymbol{\ell} \times \mathbf{r}}{r^2}$$

$$(1)$$

where I is the current in the conductor; r is the distance from the string to the point P; $\vec{r}$ is the corresponding unit vector.

For rectangular or square coils, the distance to the point in question is constant, Figure 4.2. The fundamental magnetic field strength dHi (for a straight conductor) produced by a piece of wire of length dx is:

$$dH_i = \frac{1}{4\pi} \frac{I\cos(\theta)\,dx}{r^2} = \frac{1}{4\pi} \frac{I\cos(\theta)\,d\theta}{r^2}$$

$$(2)$$

Calculated for the whole round of square wire (considered as made up of 4 straight pieces of wire): $H = 4Hi$ (3)

4.1.2. Computational model of the magnetic field of a planar coil

The model of a integrated microfluidics with a planar coil to generate the magnetic field is shown in Figure 4.3(a). Due to the geometrical symmetry, the magnetic field is only calculated by the coil at the half position of the longitudinal cross-section of figure OABC and perpendicular to the coil, Figure 4.3 (b). In 2D simulation, the length of each wire is assumed to be infinite compared to the working distance.

Figure 4.3. (a). Magnetic trap module model using flat coils; (b). Magnetic field calculated position according to the distance to the surface of the coil.
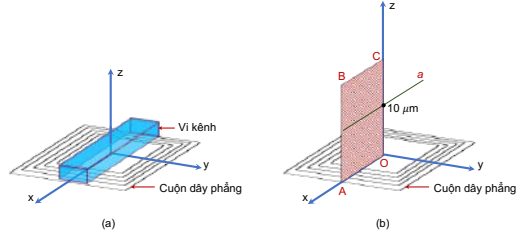
The input parameters of the coil used for calculation are described in Figure 4.3, and Table 4.1:

Table 4.1. Input parameters for calculating the magnetic field simulation of planar coils.

No	Input parameters	Values
1	Planar coil shape	Square
2	Material	Copper (Cu)
3	External radius of the coil (R_{ex})	5 mm
4	Internal radius of the coil (R_c, μm)	Depending on the number of turn (N)
5	The height of the coil (h)	15 μm
6	The space between 2 copper wires (s)	10 μm
7	The width of a copper wire (L)	10 or 15 μm
8	Number of turn (N)	50; 75; 100; 120; or 150

4.2. The results of calculation and simulation of the magnetic field of the planar coil

The strength of the magnetic field will decrease (the corresponding magnetic force acting on the magnetic particle also decreases) with long distant away from the surface of the coil. Therefore, the simulation and magnetic calculation of the coil will focus on the calculation results at the closest possible distance to the coil surface (line a in Figure 4.3). Magnetic field results at lines b; c and d (Figure 4.3) will also be given. Results of calculating magnetic field at lines a; b; c and d (Figure 4.4) are the most significant results to be discussed. Calculation results include: Fixed

parameters: Dimensions of Rex coil = 5 mm; Wire height h = 15 μm; Distance between wires s = 10 μm; Variable parameters: Conductor width L = 10 and 50 μm; Number of turns N = 50; 75; 100; 120; 150 turns.

4.2.1. Calculation results of the magnetic field of a conductor with L = 10 μm.

Fixed input parameters: The amperage applied to the coil is assumed to be I = 1 A; Rex = 5 mm; h = 15 μm, s = 10 μm. The value of the magnetic field is calculated at the position of lines a; b; c and d, Figure 4.6(b).
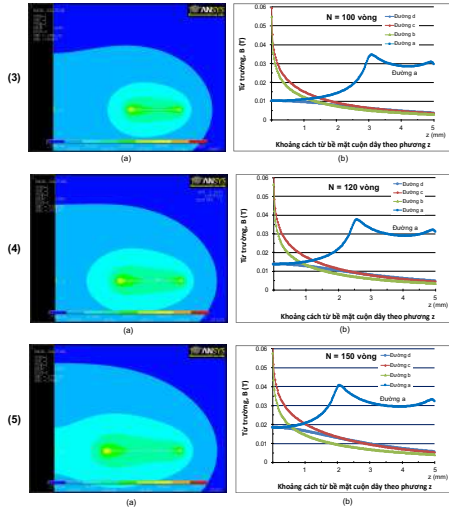

Figure 4.6. (a). The flux density generated on the coil surface; (b) The magnetic field at lines a, b, c, d corresponds to L = 10 μm; I = 1 A; Rex = 5 mm; h = 15 μm, s = 10 μm; N = 100; 120; 150 rounds.

Figure 4.6 gives the results: the flux density is extracted along the cross-section at the center of the planar coil, as shown in Figure 4.4(a). It can be seen that the flux density (corresponding to the magnetic force to capture between the magnetic nanoparticles) decreases as the distance to the coil surface gets farther away at the b lines; c and d, Figure 4.6 (b). In addition, from the results of the calculation of the magnetic field at line a, Figure 4.6 (b), it is shown that, as the number of turns of the wire increases, the magnetic field becomes stronger (corresponding to the "line a" figure (b) of the figure (1) - (5) in Figure 4.6.).

4.2.2. Calculation results of magnetic field with conductors: L = 15 μm.

The calculation results are as follows: Fixed input parameters: The current applied to the coil is assumed I = 1 A; Rex = 5 mm; h = 15 μm, s = 10 μm.

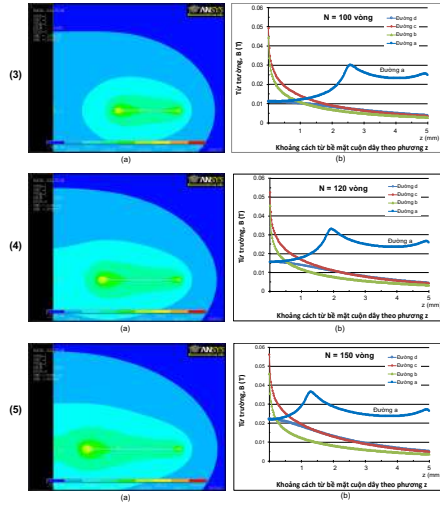*Figure 4.8. (a). The flux density generated on the coil surface; (b) The magnetic field at the lines a, b, c, d corresponds to: L = 15 μm; I = 1 A; Rex = 5 mm; h = 15 m, s = 10 μm; N = 100; 120; 150 rounds.*

Figure 4.8 shows: the magnetic field strength increases according to the turns number of the wire increases. This is similar to the result obtained when the width of the winding conductor is 10 μm. However, with the same number of turns (N) the magnetic field strength of the smaller wire will give a larger magnetic field. In addition, the lager wire will increase the coverage of the conductor on the coil surface. For the purpose of creating space on the coil surface to obtain two magnetic nanoparticle trapping zones and convenient for simple connection and fabrication the coils, the coil design will choose a design with a smaller size of the wire.

4.2.3. Calculation results of power consumption in the coil

The power consumed in the coil will be calculated corresponding to the parameters of wire that are input parameters of the simulation of magnetic field calculations based on the Joule effect, Table 4.2.

Table 4.2. Power consumption in coil: $\rho_{Cu} = 1.68 \times 10^{-8}$ (Ω.m); L = 10 and 15 μm; I = 0.05 and 1 A corresponds to $J = 6.67 \times 10^9$ and 5.00×10^8 A/m^2.

	L = 15 (μm)				L = 10 (μm)			
			P (W)				P (W)	
STT	N (turn)	V (m³)	I = 1 (A)	I = 50 (mA)	N (turn)	V (m³)	I = 1 (A)	I = 50 (mA)
1	50	2.93×10^{-10}	218.73	1.23	50	1.78×10^{-10}	59.14	0.15
2	75	3.44×10^{-10}	257.10	1.44	75	2.66×10^{-10}	88.26	0.22

3	100	5.70×10^{-10}	426.25	2.40	100	3.53×10^{-10}	117.08	0.29
4	120	6.77×10^{-10}	506.12	2.84	120	4.39×10^{-10}	145.60	0.36
5	150	8.33×10^{-10}	622.56	3.50	150	5.24×10^{-10}	173.82	0.43

The result: the smaller the wire size, the more power is consumed. The power dissipation in the size coil $L = 10$ μm is larger than that of the coil with $L = 15$ μm. However, if the current applied to the coil is small, the heat release from the coil according to the Joule Lenz effect is not much.

4.3. Fabrication of planar coils for the module of magnetic trapping.

The fabrication process as following steps: (1) Design of coils; (2) Fabrication of masks for photolithography; (3) Fabrication mold; (4) Fabrication of coil; (5) Finish and connect coils with the support system, Figure 4.13.

Figure 4.13. Fabrication process of planar coils. (1). Create Ti/Cu seed layers on the Si subtrate. (2). Mold fabrication for the coil (by AZ4562). (3). Development. (4) Electrolysis of Cu wire. (5). Remove AZ4562. (6). Remove the Ti/Cu seed layer by dry etching.
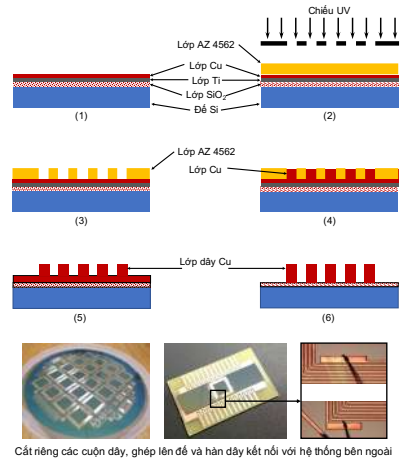
Figure 4.14. Completed coils on subtrate.

Dimensions of Cu wire: Design: width × high: 10×15 μm, parameters measured by measuring method Stylus profilometry: 10.8×5.13 μm.
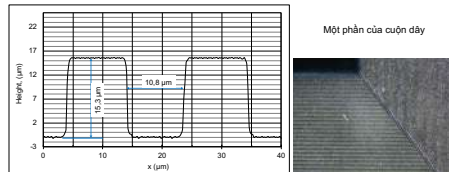

Figure 4.15. Determination of the geometrical dimensions of the Cu conductor of the coil by means of Stylus Profilometry.

4.4. Research results of Integral microfluidic system's ability to capture magnetic nanoparticles

4.4.1. Effect of curent applied to a planar coil on the temperature in the microfluidic system.

In this study, the temperature in the microfluidics was measured by small temperature sensor (K-type, 0.5 mm tip diameter) that was integrated right on top of the PDMS microchannel, as shown in Figure 4.16.

Figure 4.16. Describes integrating the temperature sensor on top of the microchannel;

Figure 4.17. Experimental diagram to study the temperature change of a planar coil when a current (DC) is applied to the system.

The temperature sensor was integrated onto the top of the microchannel during the microchannel fabrication process (as described in Section 2.2. Chapter 2), Figure 4.17. Temperature is recorded with a digital K- type temperature sensor during a current applied to the coil. This current is controlled by a linear DC source. Two experiments were performed including: Experiment 1: Measure the temperature in the microchannel that is worked with liquid being injected into the channel by a flow pump (25 µL/min of flow rate); Experiment 2: Measure the temperature in the microchannel that is worked without liquid injected into the microchannel.

The results also show the ability of the coil to work in different applications: (1). If it is necessary to generate a high magnetic field and low operating temperatures, a coil with a large number of turns will be suitable. (2). If it is necessary to generate a medium magnetic field and heat up the liquid in the microchannel, coils with fewer turns are used.

Figure 4.18 show that the temperature inside the microchannel in these two experiments has the same rate of temperature variation.
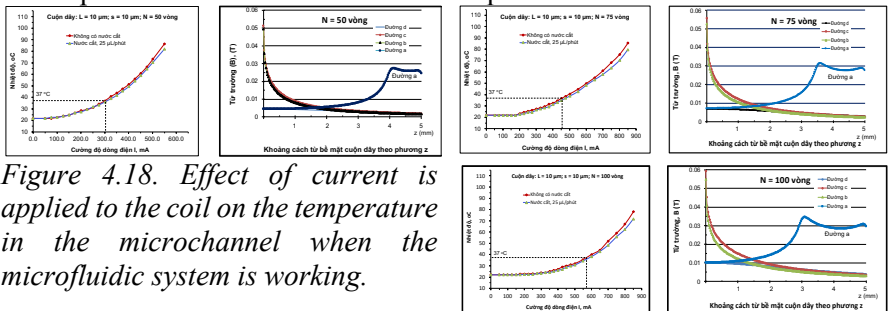

Figure 4.18. Effect of current is applied to the coil on the temperature in the microchannel when the microfluidic system is working.

4.4.2. Research on the effect of current on the ability to trap magnetic nanoparticles.

4.4.2.1. Investigation of magnetic nanoparticle trapping ability.

In this study, commercial magnetic particles, Dynabeads® MyOne™ Carboxylic Acid, with a diameter of 1.05 µm, were used to investigate the ability to trap magnetic nanoparticles by planar coils.

Pump (1) injects PBS solution (at a flow rate of 10 µL/min) into the microchannel for 1 minute for wetting the channel surface. This step is very important and necessary to limit the adhesion of particles on the channel surface and eliminate the possibility of foaming inside the channel during the experiment. Then, pump (2) injected the magnetic nanoparticles dispersed in PBS solution (mass concentration 10 mg/L) at a flow rate of 2 µL/min. The two pumps operate alternately during the magnetic nanoparticle trapping test, for example, in the first step, pump (1) is on, pump (2) is off. On the contrary, pump (2) is on and pump (1) is off. At the magnetic

Figure 4.20. Diagram of the experiment of trapping magnetic nanoparticles.

nanoparticle trapping zone, the nanoparticles are observed by a digital microscope (KEYENCE VHX - 1000 digital microscope). The parameter of microchannels in this experiment are linear with two inputs. The width of the microchannel is 250 µm, 50 µm high and 4.5 cm long. The parameter of planar coils are: 1 cm of width; 75 turns, 10x10 µm of Cu wire. Current applied to the coil are I = 0; 60; 100; 200; 300; 400; 500 mA with the voltage of 1.5 - 2 V. The results on the ability trapping of magnetic nanoparticle of the planar coil are shown in Figure 4.21.
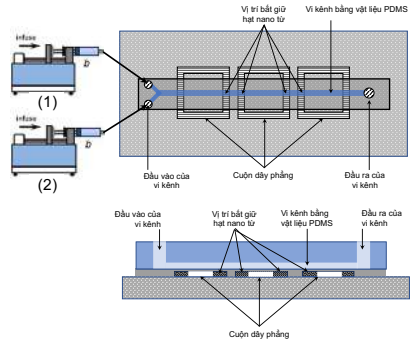
Figure 4.21. Trapping magnetic nanoparticles in the the microfluidic chip with 250 µm microchannel, at current applied (I): (a) I = 0 mA; (b) I = 100 mA; (c) I = 300 mA, (d) I = 0 mA. (e) Microfluidic with microchannel 250 µm wide, 50 µm high and 4.5 cm long. Flow rate: 2 µL/min

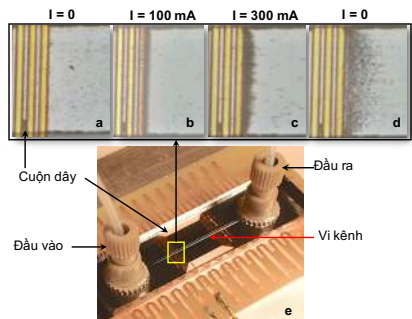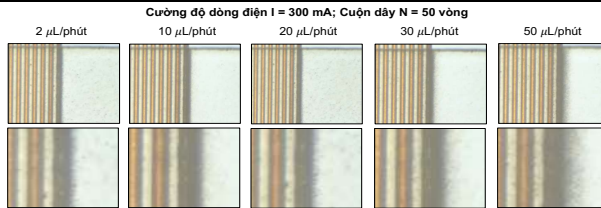

Figure 4.21 (a - d) shows that when current is applied to the coil (I = 100 and 300 mA), the magnetic particles are trapped at the conductors (Figure 4.21.(b, c)). At a higher current the trapping ability of nanoparticles is better. When the current is turn off, magnetic particles are released from these wires.

4.4.2.2. Effect of the flow rate in microchannel on the magnetic nanoparticle trapping ability.

In this section, the effects of flow rate on the trapping ability of magnetic nanoparticles in the microfluidics are investigated based on the current applied to the coils 300 and 570 mA, respectively, and coil with 50 and 100 of turn number. Experimental parameters are given in Table 5.3.

Table 5.3. Experimental parameters for study the effect of liquid flow rate in the microchannel on the trap of magnetic nanoparticles.

Flow rate in micro-channel, µL/min	Turn number N = 50 turns	Turn number N = 100 turns
2 µL/min	I = 300 mA	I = 570 mA
10 µL/min	I = 300 mA	I = 570 mA
20 µL/min	I = 300 mA	I = 570 mA
30 µL/min	I = 300 mA	I = 570 mA
50 µL/min	I = 300 mA	I = 570 mA

Cường độ dòng điện I = 300 mA; Cuộn dây N = 50 vòng

2 µL/phút	10 µL/phút	20 µL/phút	30 µL/phút	50 µL/phút

CHAPTER 5. INTEGRATING ELCTROCHEMICAL SENSOR INTO MICROFLUIDIC SYSTEM APPLICATIONS FOR ANTIBIOTIC ANALYSIS.

In this section, the research results are shown the fabrication of microfluidic chip integrated with electrochemical sensors, and the appication this chip in determining the antibiotic Sulfamethoxazole used in livestock.

5.1. Design of microfluidic chip integrated with modified screen-printed electrode (SPE)

5.1.1. Microfluidic chip design

After fabricating microchannel systems using PDMS materials, microfluidic chips with SPE are designed and fabricated as described in Figure 5.3. The electrochemical sensor integrated
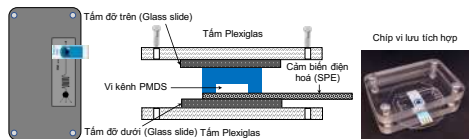

Figure 5.3. Description of integrating the electrochemical sensors (SPE) to microfluidic systems.

into the microfluidic system is performed by the reversible bonding technique.

5.1.2. Assembling microfluidic chip into the experimental system

The experiments are designed by assembling the microfluidic chip with micropump, electrochemical measurement system as shown in Figure 5.5.
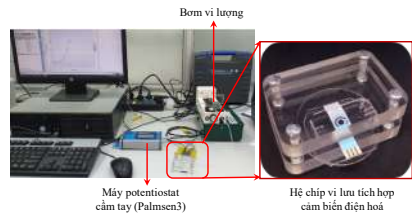

Figure 5.5. The chip integrates the SPE electrode and the electrochemical measurement system.

5.2. Fabrication of a modified electrochemical sensor based on the SPE electrode.

5.2.1. The materials for modifying the SPE

In this study, the rGO/PDA-CuNPs materials (in which: rGO - reduced Graphene oxide); PDA - polydopamine; CuNPs - copper nanoparticles) were electrochemically synthesized on the electrode surface. Then this modified SPE was selected for analyzing the sulfonamide antibiotics. In particular, the copper nanoparticles (CuNPs) is play as a role as an electrochemical catalyst for the oxidation of sulfamethoxazole (SMX) on the electrode surface. The polydopamine layer (PDA) will make the bonding the carbon material of the working electrode to the CuNPs by the -OH or -NH functional groups. Figure 5.7 shows the process of modification of the carbon working electrode surface of the SPE with the materials by direct synthesis on the working electrode.

Figure 5.7. Schematic diagram of the steps to modify the surface of SPE electrode by rGO/PDA-CuNPs materials.
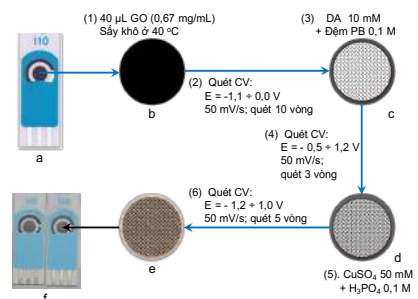
To confirm the successful surface modification of SPE electrode by the above procedure, this modification was carried out simultaneously on glassy carbon electrode (GCE - glass electrode - carbon) for comparison.

5.2.2. Survey results on fabrication conditions of rGO/PDA-CuNPs material system on glassy carbon electrode (GCE).

5.2.2.1. Synthesis of rGO by electrochemical method

Figure 5.9 shows the CV signal from the process of reduction of GO on the surface of the GCE electrode. The results shows that there is a peak

appears at a value of about -0.25 V of the first CV circle, which proves that the GO is electrochemically reduced to rGO on surface.

Figure 5.9. CV spectrum of the reduction process of GO on the GCE/GO electrode in 0.2M PB buffer with potential scanning speed 50mV/s, and 5 circles of scanning.
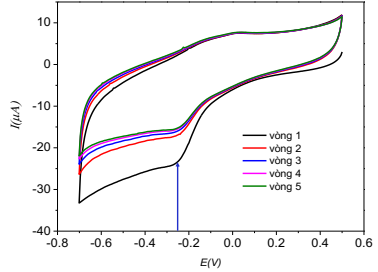
To test this electrode activity in determining the concentration of SMX with the concentration of 40 µM, when scanning the potential in the range 0.4 to 1.2 V according to the square pulse scanning (SWV) technique of both two modified GCE and GCE electrodes. The results are shown in Figure 6.11, there is a peak at 0.9V according to the specific signal of SMX using the GCE/rGO electrode higher than this signal that uses the GCE electrod. In addition, the conductivity of the GCE/rGO electrode is better than the GCE original electrode.
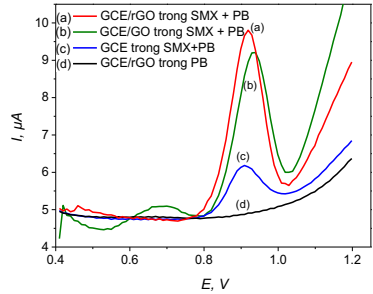
5.2.2.2. Synthesis of polydopamine layer on GCE/rGO electrode

The polydopamine (PDA) polymerization results are shown in Figure 5.12. The signal after each circle is moved folow the direction of the arrow.

Figure 5.12. The CV signal of PDA layer on GCE/rGO electrode with 9 scanning cycles, scanning speed of 50 mV/s, DA concentration of 10 mM in 0.2 M PB buffer.

Figure 5.11. SWV signal of (a) GCE/rGO, (b) GCE/GO, and (c) GCE bare electrode with 40 µM SMX, (d) GCE/rGO electrode in 0.2M PB buffer.
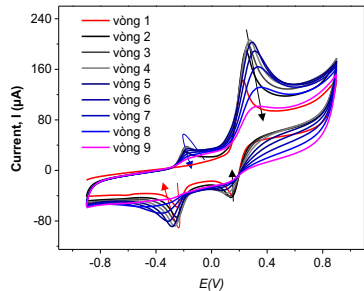
With 9 of scanning cicles, the conductivity of the electrode decreases, leading to a decrease in the polymerization process speed because the PDA layer is not conductive. Therefore, the experiment of investigating the effect of the number of potential scan cycles on the PDA synthesis on the electrode stopped at 9 cycles. After successfully synthesizing the PDA layer on the surface of the GCE electrode, this electrode was used to test the determination of SMX in PB buffer by SWV square wave scanning method to evaluate the efficiency of this electrodes coated with PDA film, Figure 5.14

Figure 5.14. The SWV signal of the GCE/rGO/PDA electrode with SMX 40 µM +PB and buffer PB has 3,6.9 turns of PDA membrane synthesis; sweep potential range from -0.4 V to 1.2 V; scanning speed of 50 mV/s.
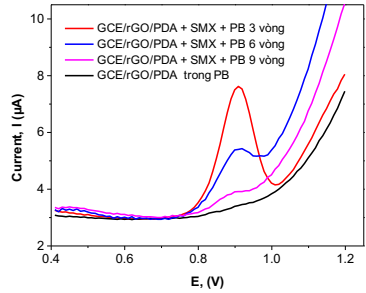
5.2.2.3. Results of the synthesis CuNPs on GCE/rGO/PDA electrode

Copper nanoparticles (CuNPs) were synthesized onto the surface of the GCE/rGO/PDA electrode by using a CuSO₄ 3 mM solution in H₃BO₃ 0.1 M at a potential range of -1.2 V to +1.0 V with 5 circles of scanning and 30 mV/s of scanning speed. Figure 5.15 shows the CuNPs synthesis process on the surface of GCE/rGO/PDA electrode, there are a pair of redox peaks at the +0.5V/-0.4V of Cu/Cu^{2+} on the electrode surface. The GCE/rGO/PDA electrode system was then used to detect 40 µM SMX in 0.2 M PB buffer.
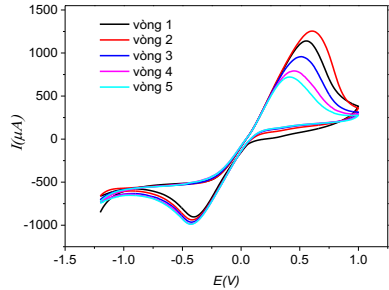

Figure 5.15. CV signal of the CuNPs synthesis on GCE/rGO/PDA electrode in $CuSO_4$ 3mM + H_3BO_3 0.1M solution at potential range -1.2 V to + 1.0 V; 5 cycles of scanning, and 30 mV/s scanning speed.

Figure 5.16. SWV signal of electrodes (a) GCE/rGO/PDA-CuNPs, (b) GCE/CuNPs and (c) electrode GCE with 40 µM SMX, (d) PB buffer 0.2 M; Potential ranges from -0.4 V to 1.2 V; potential scanning speed 50 mV/s; 3 circles of scanning.
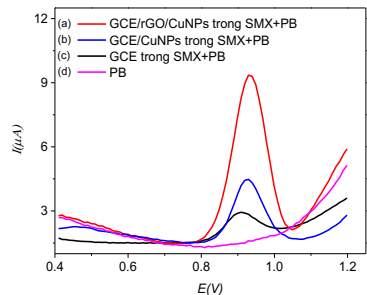
Optimal conditions of materials synthesis on GCE electrode surface as flowing: For rGO: Potential range from -0.7 to 0.5 V; scanning speed 50mV/s, 5 circles; For PDA: Voltage range from -0.9 V to +0.9 V, scanning speed 50mV/s, 3 circles; For Cu nanoparticles (CuNPs): potential range -1.2 V to +1.0 V; scanning speed 30mV/s; 5 circles. These conditions are used for modifying the working electrode surface of the screen-printed electrode.

5.2.3. Surface modification of SPE electrode by rGO/PDA-CuNPs materials.

5.2.3.1. The results of rGO synthesis by electrochemical method on the surface of SPE electrode.

The condition of graphene oxide modified SPE electrode was similar to that performed on the GCE electrode and in the same sequence as shown in Figure 5.17. Figure 5.17. shows the CV spectral signal of the reduction of GO on the surface of the SPE electrode. There is a strong reduction peak at the potential value of -0.63 V at the first potential circle. This peak is proved that there is an electrochemical reduction of GO to rGO. In next circle,

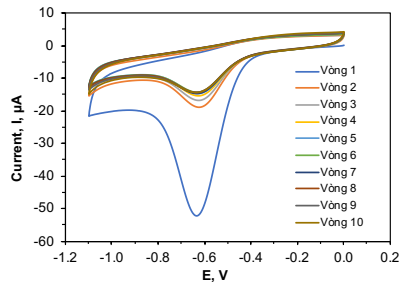*Figure 5.17. CV spectrum of GO reduction of SPE electrode in PB buffer 0.2M, Na_2SO_4 0.1 M. Scanning speed 50mV/s, 10 cycles.*

the peak of GO reduction to rGO still maintained and stabilized the reducing current intensity value at about -18 to -15 μA.

However, the reduction potential value on the SPE electrode is larger than that on the GCE electrode. This result is possible thanks to the porosital surface of the SPE electrode, and the conductivity of the powdered carbon has a greater internal resistance than that of the GCE electrode.

5.2.3.2. The results of PDA synthesis by electrochemical method on the surface of SPE/rGO electrode.

Carry out the polymerization of PDA from DA 10mM solution + 0.2 M PB (pH = 6) + Na_2SO_4 0.1 M solution by scanning 8-circles of CV at the potential range from -0.5 V to + 1.2 V, scanning speed 50mV/s. Figure 5.18 shows PDA polymerization results.

Figure 5.18. CV signal of PDA layer polymerization on SPE/rGO electrode with 8 scanning cycles, scanning speed 50 mV/s, DA 10 mM in 0.2 M PB buffer (pH = 6), Na$_2$SO$_4$ 0 ,1 M.
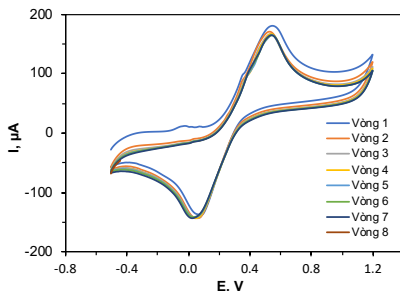
5.2.3.3. Synthesis of Cu nanoparticles by electrochemical method on the surface of SPE/rGO/PDA electrode.

Cu nanoparticles (CuNPs) were synthesized onto the surface of SPE/rGO/PDA electrode by using the CuSO$_4$ 3 mM solution in H$_2$SO$_4$ 0.1 M at the potential range of -1.2 V to +1.0 V with 5 circles of scanning and scanning speed of 30mV/s. Figure 6.19 shows a stable oxidation/reduction peak at about 0.58 V and - 0.84 V of Cu/Cu^{2+} on the surface of the SPE electrode, Hình 5.19.

Figure 5.19. CV signal of CuNPs synthesis on SPE/rGO/PDA electrode in CuSO$_4$ 3mM + H$_2$SO$_4$ 0.1M solution at potential range -1.2 V to + 1.0 V; 5 cycles of scanning, scanning speed 30 mV/s.
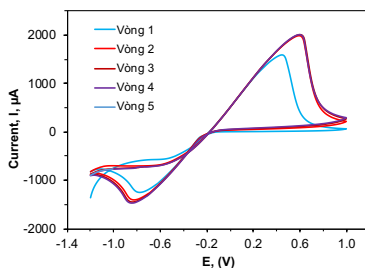
5.2.4. Electrochemical characteristics of rGO/PDA-CuNPs material system on the surface of SPE electrode.

To estimate the electroactive surface area of the electrode, a CV scanning of the SPE/rGO/PDA-CuNPs; SPE/CuNPs; SPE/rGO/CuNPs and SPE/PDA-CuNPs electrodes in K$_3$Fe(CN)$_6$/ K$_4$Fe(CN)$_6$ 5 mM and KNO$_3$ 1M from -0.15 V to +0.5 V with scanning speed from 10 to 150mV/s, Figure 5.20. According to the Randles-Sevcik equation, the peak intensities of the anodic and cathode bias currents (Ipa and Ipc) will be proportional to the square root of the potential sweep rate.

$$Ipa = (2.69.10^5).n^{3/2}.A.D^{1/2}.C.v^{1/2} \qquad (3.1)$$

Experimental and calculated results show that the electroactive surface of the SPE/rGO/PDA-CuNPs; SPE/CuNPs; SPE/rGO/CuNPs and SPE/PDA-CuNPs electrodes are given in Table 6.1. The results show that the presence of PDA reduces the electrical conductivity of the material system while the presence of rGO increases the efficiency of the material.
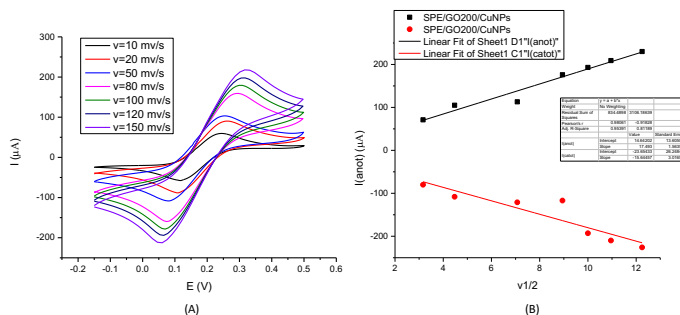
(A)   (B)

Figure 5.20. (A) CV polarization curve of GCE/rGO/PDA-CuNPs electrode in $K_3Fe(CN)_6$/ $K_4Fe(CN)_6$ 5mM solution mixed in KNO$_3$ 1M at scanning potential rates 10 - 120 mV/s. (B) Regression curve of the dependence of the anode peak intensity I_{pa} and the cathode peak on the scanning potential rate $v^{1/2}$

Table 5.1. Electroactive surface area of SPE-based electrodes.

Electrode	Electroactive surface area, (mm²)
SPE	12.5
SPE/rGO/PDA-CuNPs	19,1
SPE/CuNPs	18,8
SPE/rGO/CuNPs	16,1
SPE/PDA-CuNPs	11,8

5.2.5. Morphological and structural characteristics of rGO/PDA-CuNPs material on the surface of SPE electrode.

The synthesized material system was evaluated for composition and surface structure by the results of SEM image analysis, EDX spectrum, FT-IR spectrum. The results of surface composition analysis of the material system are shown in Figure 5.21 from EDX spectroscopy.


Figure 5.21. EDX spectrum of the SPE/rGO/PDA-CuNPs electrode system.

Figure 5.22. SEM image of the electrode surface (A) SPE/rGO/PDA-CuNPs; (B) SPE/rGO/PDA; (C)SPE/rGO; and (D) SPE.

(A)   (B)

(C)   (D)
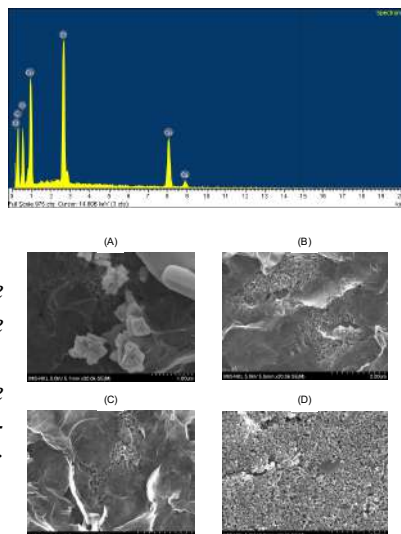
The presence of CuNPs nanoparticles and PDA films on surface of SPE elctrode is confirmed through EDX results, and SEM images Figure 5.22. The results showed that on the SPE/rGO/PDA-CuNPs electrode, the Cu content accounted for 3.88% (atomic), which confirmed the presence of Cu on the electrode surface.

Figure 5.23. FTIR infrared spectra of rGO/PDA/CuNPs; rGO/CuNPs; rGO/PDA and GO material.
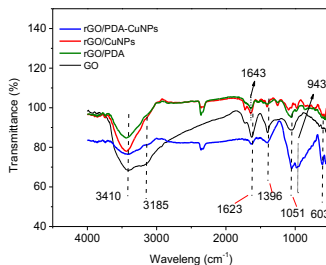
The FTIR spectrum shows the GO has a peack signal of a carbonyl group – C = O at 1623 cm^{-1}. The peak at 1396 cm^{-1} characterizes the existence of a C–O bond. The peak at 1643 cm^{-1} characterizes the existence of a C = C bond, while the peak at 1051 cm^{-1} represents the C-O-C bond. In addition, the peak 3410 cm^{-1} is typical for the presence of -OH groups. The PDA synthesis is successful as shown by the characteristic peak of the NH bond at 1643 cm^{-1}. In addition, the peak at position 603 cm^{-1} is assigned to Cu-O bond, due to interaction between CuNPs with OH group of polydopamine or with – COOH group still in rGO. It is proved that the role of PDA in the electrolysis of CuNPs precipitate on the electrode surface.

When studying the wettability of the materials on the electrode surface with different layers, the wettability change is caused by these material systems, and these material layers have good contact with solution during the analysis process, Figure 5.24.

Figure 5.24. Contact angle (θ) of the electrode surfaces (a) original SPE, (b) SPE/rGO, (c) SPE/rGO/PDA, (d) SPE/rGO/PDA-CuNPs.
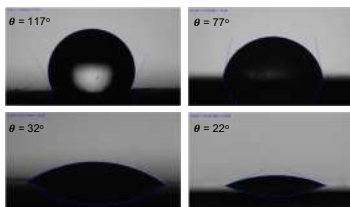
5.3. Application of microfluidic chip integrated with modified screen-printed electrode in determining sulfamethoxazole antibiotic residues.

Determination of sulfamethoxazole (SMX) in PB buffer was carried out by microfluidic system integrated with SPE electrode modified by rGO/PDA-CuNPs materials. The standard curve is built based on the serials of SMX concentration which were prepared from the standard solution with 4 – 1000 µM of concentration, Figure 5.25. The real sample of sulfomethoxazone was prepared from the commercial antibiotic of Nam

Thai veterinary drug company – T.T.S (contains Sulfamethoxazole 20 g/100g and Trimethoprim 4.0g/100g), Figure 5.26. Figure 5.25 shows that a linear response in the concentration of SMX is ranged of 4 to 200 µM, thereby, the limit of detection (LOD) for SMX is determined about 1.5 µM. The signal of the SMX detection in commercial drug samples (T.T.S) is significant and certain accuracy with recovery coefficient of 98.5%. After each measurement, to reuse the eleectrode, a precess is caried out as flowing step: the microfluidic chip was injected with PB buffer solution to wash and scanned electrodes by SWV method to remove SMX after analysis. The electrode could be reused at least 5 times, and the electrode is remained stable. To check the cleanliness of the microfluidic chip (in SMX removal after washes), the chip was injected with PB buffer, and then the SWV scan again. The results show that there is no existence of SMX peak after washing channel and electrode two times.
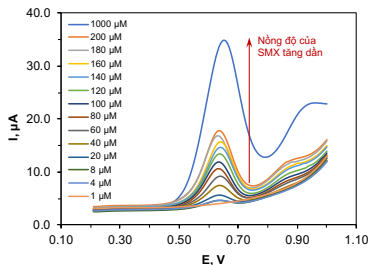
Figure 5.25. Current signal by SWV method of SPE/rGO/PDA-CuNPs electrode when determining SMX with concentration varying from 1 to 1000 µM, in 0.2 M PB buffer; The sweep potential range is from 0.2 to 1 V; scanning speed of 50 mV/s.

In addition, the initial test with the drug sample of SMX (prepared from T.T.S product) is carried out at two concentration of 20 and 40 µM. The drug was dissolved in PB buffer, then injected into the microfluidic system at a flow rate of 10 µL/min. the result is shows in Figure 5.26.

Figure 5.26. Square wave pulse (SWV) current signal of the SPE/rGO/PDA-CuNPs electrode when determining the SMX with two concentrations of 20 and 40 µM, in 0.2 M PB buffer; The sweep potential range is from 0.2 to 1 V; scanning speed of 50 mV/s.
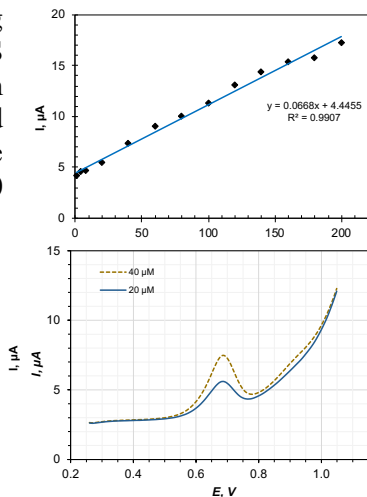
CONCLUSIONS AND RECOMMENDATIONS

I. CONCLUSION:

1. The design of the planar coil was carried out and the magnetic field generated by the coil was calculated. The coil is electro-magnet that can be integrated with the microfluidics to build an integrated chip for the purpose of trapping magnetic nanoparticles for bioanalytical applications by ELISA analysis technique.

2. Development of the package mcirofluidic chip by mechanical packing technique, and microfluidic chip can be used in many times, especially the substrate system. Therefore, this technique helps to save the cost and time of fabricating the integrated microfluidic chip. In addition, the chip can be reused in many times compared to the method of packing chip by using plasma technology.

3. Coils with different size were tested to trap magnetic nanoparticles with size 1.0 μm with flow rate of liquid in microchannels up to 100 μL/min.

4. Design and fabricate a special micro-controller valve system for microfluidic systems. This microvalve can manuplated multi-flow of liquids injected into the microchannel and saved costs compared to commercial valve systems.

5. Design and manufacture a microfluidic chip integrated with a flat electrochemical sensor for the purpose of analyzing the antibiotic content of sulfomethazone in antibiotics used in livestock

II. NEXT RESEARCH ORIENTATION

1. Optimizing the fabrication of planar coil with smaller size.

2. Optimizing of magnetic nanoparticle trapping and complete the implementation of ELISA technique in microfluidic chip system.

3. Optimizing of electrochemical sensor integration technique on various SPE planar electrodes.

4. Optimizing the modification the electrochemical sensor with advance materials and taking the analyst antibiotic with lower concentration by using the integrated microfluidic chip system.

5. Optimizing antibiotic analysis with optimization of repeatability, stability, limit of detection (LOD, LOQ) and sensor specificity.

THE RESULTS AND NEW CONTRIBUTIONS OF THE THESIS:

1. The design and simulation process of the magnetic field generated by the planar coil has been executed, representing a novel advancement in magnetic field calculation and coil design. As a result, the planar coils have been successfully manufactured and utilized as trapping coils integrated into a microfluidic system to create an integrated chip for biological analysis using ELISA analysis techniques. Experimental tests were conducted to capture nanoparticles with a size of 1.0 μm, and the trapping process demonstrated high efficiency, with a liquid flow rate in the microchannel reaching up to 100 μL/h. This was achieved by applying a current of up to 570 mA to the coils while maintaining a temperature below 37°C.

2. A new technique has been developed to improve the reusability of microfluidic systems. By using a mechanical structure, the microchannels can be reused multiple times, unlike the traditional method of immobilizing microchannels using plasma techniques. This development has helped reduce the cost and time required to manufacture integrated microfluidic chip systems.

3. A specialized control valve system has been designed and manufactured for the microfluidic system. This valve system allows for simultaneous control of multiple liquid streams pumped into the microfluidic device while also reducing costs compared to commercial valves. This development is a significant step towards efficiently operating the microfluidic system in Vietnam.

4. Design and manufacture a microfluidic chip integrated with a flat electrochemical sensor for the purpose of analyzing the antibiotic concentration of Sulfomethazone used in livestock. This achievement is a starting point for designing and improving integrated microfluidic systems to analyze different substances.

PUBLICATIONS

1. T.N. Le, V. A. Nguyen, G.L. Bach, L.D. Tran, H.H. Cao, Design and Fabrication of a PDMS-Based Manual Micro-Valve System for Microfluidic Applications, Advances in Polymer Technology, 2020, p 1.

2. Tu Le Ngoc, Nguyen Cong Thinh, Lam Dai Tran, Van-Anh Nguyen, Ha Cao Hong, Microfluidic chip for trapping magnetic nanoparticilesand heating in terms of biological analysis, Communications in Physics, 30 (2020) p 245-256.

3. Le The Tam, Nguyen Hoa Du, Le Trong Lu, Nguyen Thi Hai Hoa, Le Ngoc Tu, Tran Dai Lam, Magnetic resonance imaging (MRI) application of fe3o4based ferrofluid synthesized by thermal decomposition using poly (maleic anhydride - alt-1-octadecene) (PMO), Vietnam Journal of Science and Technology, 56, 1A (2018), p 174-182.

4. Lê Ngọc Tú, Trần Đại Lâm, Nguyễn Phúc Quân, Nguyễn Vân Anh, Lê Trọng Huyền, Cao Hồng Hà, Tổng hợp vật liệu nanocompozit trên cơ sở graphen oxit khử, polydopamin và hạt nano đồng cho chế tạo cảm biến xác định sulfamethoxazole, Tạp chí Phân tích Hoá, Lý và Sinh học, *(accepted, No. 2, 2023).*